



FULL PAPER

Synthesis, characterization, and biological screening of metal complexes of novel sulfonamide derivatives: Experimental and theoretical analysis of sulfonamide crystal

Sajjad H. Sumrra¹ | Abrar U. Hassan¹ | Muhammad Imran² |
Muhammad Khalid³ | Ehsan U. Mughal¹ | Muhammad N. Zafar⁴ |
Muhammad N. Tahir⁵ | Muhammad A. Raza¹ | Atualpa A.C. Braga⁶

¹Department of Chemistry, University of Gujrat, Gujrat, 50700, Pakistan

²Department of Chemistry, Faculty of Science, King Khalid University, Abha, 61413, Saudi Arabia

³Department of Chemistry, Khwaja Fareed University of Engineering & Information Technology, Rahim Yar Khan, 64200, Pakistan

⁴Department of Chemistry, Quaid-i-Azam University, Islamabad, 45320, Pakistan

⁵Department of Physics, University of Sargodha, Sargodha, Pakistan

⁶Departamento de Química Fundamental, Instituto de Química, Universidade de São Paulo, Av. Prof. Lineu Prestes, 748, São Paulo, 05508-000, Brazil

Correspondence

Sajjad H. Sumrra, Department of Chemistry, University of Gujrat. Gujrat 50700, Pakistan.
Email: sajjadchemist@gmail.com

Muhammad Khalid, Department of Chemistry, Khwaja Fareed University of Engineering & Information Technology, Rahim Yar Khan, 64200, Pakistan.
Email: muhammad.khalid@kfueit.edu.pk

Funding information

Higher Education Commission (HEC), Grant/Award Number: 7800

This study reports the synthesis of sulfonamide-derived Schiff bases as ligands L^1 and L^2 as well as their transition metal complexes [VO(IV), Fe(II), Co(II), Ni(II), Cu(II), and Zn(II)]. The Schiff bases (4- $\{E$ -[(2-hydroxy-3-methoxyphenyl)methylidene]amino}benzene-1-sulfonamide (L^1) and 4- $\{[(2$ -hydroxy-3-methoxyphenyl)methylidene]amino}- N -(5-methyl-1,2-oxazol-3-yl)benzene-1-sulfonamide (L^2) were synthesized by the condensation reaction of 4-amino-benzene-1-sulfonamide and 4-amino- N -(3-methyl-2,3-dihydro-1,2-oxazol-5-yl)benzene-1-sulfonamide with 2-hydroxy-3-methoxybenzaldehyde in an equimolar ratio. Sulfonamide core ligands behaved as bidentate ligands and coordinated with transition metals via nitrogen of azomethine and the oxygen of the hydroxyl group. Ligand L^1 was recovered in its crystalline form and was analyzed by single-crystal X-ray diffraction technique which held monoclinic crystal system with space group ($P2_1/c$). The structures of the ligands L^1 and L^2 and their transition metal complexes were established by their physical (melting point, color, yields, solubility, magnetic susceptibility, and conductance measurements), spectral (UV-visible [UV-Vis], Fourier transform infrared spectroscopy, 1H NMR, ^{13}C NMR, and mass analysis), and analytical (CHN analysis) techniques. Furthermore, computational analysis (vibrational bands, frontier molecular orbitals (FMOs), and natural bonding orbitals [NBOs]) were performed for ligands through density functional theory utilizing B3LYP/6-311+G(d,p) level and UV-Vis analysis was carried out by time-dependent density functional theory. Theoretical spectroscopic data were in line with the experimental spectroscopic data. NBO analysis confirmed the extraordinary stability of the ligands in their conjugative interactions. Global reactivity parameters computed from the FMO energies indicated the ligands were bioactive by nature. These procedures ensured the charge transfer phenomenon for the ligands and reasonable relevance was established with experimental results. The synthesized compounds were screened for antimicrobial activities against bacterial (*Streptococcus aureus*, *Bacillus subtilis*, *Eshcheria coli*, and *Klebsiella*

pneumoniae) species and fungal (*Aspergillus niger* and *Aspergillus flavous*) strains. A further assay was designed for screening of their antioxidant activities (2,2-diphenyl-1-picrylhydrazine radical scavenging activity, total phenolic contents, and total iron reducing power) and enzyme inhibition properties (amylase, protease, acetylcholinesterase, and butyrylcholinesterase). The substantial results of these activities proved the ligands and their transition metal complexes to be bioactive in their nature.

KEYWORDS

biological screening, crystal structure, DFT study, sulfonamide, transition metal complexes

1 | INTRODUCTION

Coordination chemistry is gaining recognition due to extensive applications in the development of pharmaceuticals, biomedicine, clinical science, and catalysis.^[1] Several transition metal complexes as metallodrugs are found to be very effective in their mechanism of action with fewer side effects compared to their organic counterparts.^[2] Researchers have studied the structure and biological properties of metallodrugs^[3] and found that numerous nitrogen and oxygen atoms in their chelates have a complex role in imparting bioactive characteristics.^[4] Interest in developing these metal chelates from bioactive compounds stems from the fact that ordinary drugs cannot compete with pathogenic resistance accompanied by drug resistance.^[5] Such resisting behavior of pathogens demands modification and diversification of these bioactive compounds to make them compatible with current needs.^[6] Metal-based drugs are proving to be potential candidates to replace their traditionally used counterparts.^[7] This may be due to their higher yields^[8] with lower possibilities of isomer generation.^[9] Several bioactive compounds, such as sulfonamides, triazoles, isatins, and benzothiazines, have been modified structurally to cope with ever-increasing pathogenic resistance as a result of their drug resistance.^[10] Specific biological roles of transition metals are also noteworthy regarding this development.^[11] Pathogenic resistance coupled with drug resistance has posed scientists a serious challenge to design and develop such bioactive compounds.^[12] The synthesis of these compounds has been seen exponentially for the last two decades.^[13] Sulfonamide cores as biologically active candidates are widely employed as antifungal,^[14] antibacterial,^[15] antioxidant,^[16] and anticancer agents,^[17] and as insulin mimics^[18] and enzyme inhibitors.^[19] By knowing such unique properties, many such bioactive derivatives have been designed.^[20] Schiff base compounds derived from sulfonamides have been an area of interest for synthetic scientists for the last

three decades due to their bioactive roles.^[21] As a result of the pharmacological behavior of sulfonamides and transition metals, we wished to combine the chemistry of these moieties to counter drug resistance.

2 | EXPERIMENTAL

All the chemicals used were of analytical grade, purchased from Sigma Aldrich and used without any further purification. Ethanol was doubly distilled before its use. All the glassware used was washed thoroughly. The melting points of synthesized compounds were determined on a Stuart melting point (MP) apparatus (Stone, Staffordshire, UK). A Nicolet FT-IR spectrophotometer (168, third avenue, Waltham, Massachusetts, USA) was used to record the IR spectra in their spectral regions using it in its default version. ¹H and ¹³C NMR spectra (Manning road, Billerica, Massachusetts, USA) were determined using a Bruker Advance 300 MHz instrument (Thermo Electron Corporation, USA). For the mass spectrometric analysis, synthesized compounds (ligands and complexes) were dissolved in dimethyl sulfoxide (DMSO) and injected through a direct insertion pump into an LTQ XL linear ion trap mass spectrometer (Thermo Scientific, USA) equipped with an electrospray ionization (ESI) probe. A high-tech Shimadzu UV-4000 spectrophotometer (Nakagyo, Kyoto, Japan) was used to record the UV-visible (UV-Vis) spectra. Biological activities were evaluated using the recommended procedures at the Natural Product Research Laboratory, University of Gujrat, Gujrat.

2.1 | Synthesis of sulfonamide ligands L¹ and L²

The ligands were synthesized according to the previously reported method.^[22] For the synthesis of L¹, 15 ml of ethanolic solution of 2-hydroxy-3-methoxybenzaldehyde (1.52 g, 10 mmol) was refluxed continuously in a 100 ml

round-bottomed flask. After 10 min, 15 ml of 4-aminobenzene-1-sulfonamide (1.72 g, 10 mmol) was added in an equimolar ratio and the resulting reaction mixture was refluxed continuously for 8 hr. Formation of the product (**L**¹) was continuously monitored with thin-layer chromatography until a single spot of the product appeared on TLC. The precipitated product was filtered, washed with a hot solution of ethanol and ether (1:1), and recrystallized to obtain fine crystals. The same procedure was used for the synthesis of **L**² by refluxing the ethanolic solution of 2-hydroxy-3-methoxybenzaldehyde (1.52 g, 10 mmol) with 4-amino-*N*-(3-methyl-2,3-dihydro-1,2-oxazol-5-yl)benzene-1-sulfonamide (0.255 g, 10 mmol) (Scheme 1).

2.1.1 | 4-*E*-[(2-hydroxy-3-methoxyphenyl)methylidene]amino} benzene-1-sulfonamide (**L**¹)

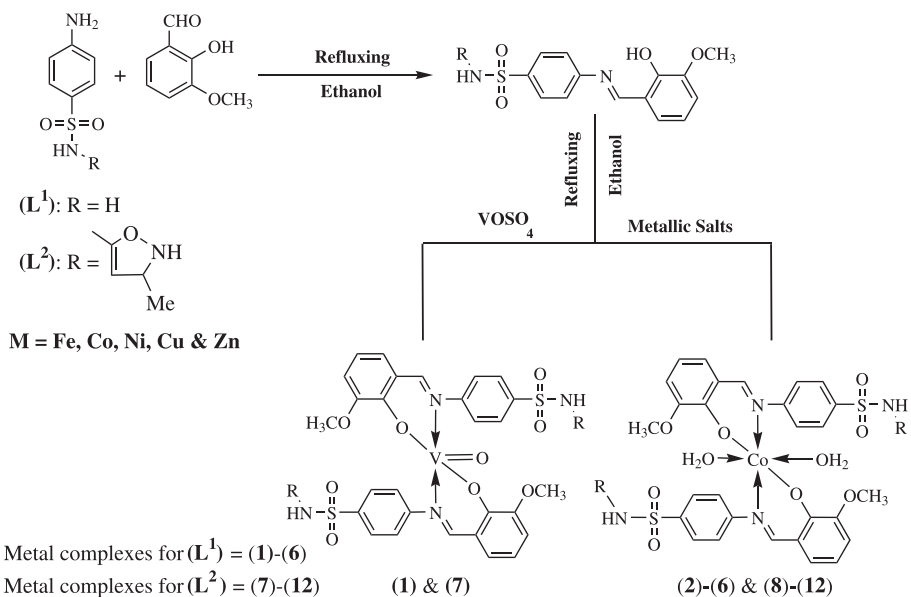
Yield: 84%, 1.26 g; MP (°C): 209; color: light red; FT-IR (cm⁻¹): 3309 (–OH), 3205 (–NH₂), 1607 (CH=N), 1312, 889 (SO₂N–H), 1155 and 1262 (O=S=O). ¹H NMR (300 MHz, DMSO-*d*₆), δ (ppm): 3.83 (m, 3H, CH₃O–Ph), 3.85 (SO₂–NH₂), 6.91–7.16 (m, 4H, N–Ph), 7.18–7.29 (m, 4H, SO₂–Ph), 8.99 (s, 1H, azomethine), 12.72 (s, 1H, OH); ¹³C NMR (300 MHz, DMSO-*d*₆), δ (ppm): 56.36 (methoxy) 116.42, 119.33, 119.71, 122.27, 124.26 127.56 (6C–Ph), 151.50 (C=N, azomethine), 165.61 (C5). MS (ESI) *m/z* (%): 306.33 C₁₄H₁₄N₂O₄S [M⁺], 123 (2.31), 136.14 (11.45), 183.08 (18.22), 226 (100), 252 (30.12), 275 (21.44). Anal. calcd for C₁₄H₁₄N₂O₄S (306.34): C (54.89), H (4.61), N (9.14); found: C, (54.63), H (4.21), N (9.24).

2.1.2 | 4-[(2-hydroxy-3-methoxyphenyl)methylidene]amino}-*N*-(5-methyl-1,2-oxazol-3-yl)benzene-1-sulfonamide (**L**²)

Yield 84%; MP (°C): 226; color: brick red; FT-IR (cm⁻¹): 3309 (–OH), 1604 (CH=N), 1345, 978 (SO₂N–H), 1162 and 1261 (O=S=O). ¹H NMR (300 MHz, DMSO-*d*₆), δ (ppm): 2.29 (s, 3H, methylisoxazole), 3.85 (SO₂–NH), 6.09 (s, 1H, isoxazole), 7.15–7.18 (m, 3H, Ph), 6.18–6.95 (m, 4H, N–Ph), 8.96 (s, 1H, azomethine), 12.51 (s, 1H, OH); ¹³C NMR (300 MHz, DMSO-*d*₆), δ (ppm): 12.52 (methylisoxazole), 56.36 (methoxy) 95.1, 95.88, 113.03 (3C–isoxazole), 116.56, 119.37, 119.72, 120.52, 122.71, 124.21 (6C–Ph), 158.41 (C=N, azomethine), 169.6 (C5). MS (ESI) *m/z* (%): 387.09 C₁₈H₁₇N₃O₅S [M⁺], 361.37 (2.31), 259.28 (21.32), 226.25 (100), 182.19 (8.4), 150 (7.89). Anal. calcd for C₁₈H₁₉N₃O₅S (389.43): C (55.52), H (4.92), N (10.79); found: C (55.12), H (4.23), N (10.19).

2.2 | Synthesis of coordination complexes 1–12

Metal complexes were synthesized by taking the ligand to metal ratio as 2:1, adopting the previously reported procedure.^[23] The respective metallic salt (50 mmol) was added to a magnetically refluxing (100 mmol) ethanolic solution of the ligand. The reaction mixture was refluxed for 4–6 hr until the product precipitate formed. The precipitated product was filtered and washed with hot ethanol. The recrystallization of product was carried out using a mixture of ethanol and ether to obtain pure product.



SCHEME 1 Synthesis of sulfonamide ligands **L**¹ and **L**² and their transition metal complexes 1–12

2.2.1 | SC-XRD studies

Single-crystal X-ray diffraction technique (SC-XRD) results were gathered by operating an APEX II CCD Bruker Kappa diffractometer at 296 K equipped with a graphite monochromator. PLATON software was used to calculate the geometric parameters (bond angles, bond distance, hydrogen bonds, and torsion angles).^[24] Crystal constructions, figures, and other mechanical information were found using Mercury 3.7 software.^[25]

2.2.2 | Computational procedures

Computational studies were performed using Gaussian 09 software.^[26] UV-Vis analysis was done by B3LYP/6-311+G(d,p) approximation^[27] in the gas phase. The results of the output files were viewed by the Gauss view, Chemcraft and Avogadro programs.

2.2.3 | Biological evaluation

Antibacterial bioassay

Ligands and their respective transition metal complexes were evaluated for their antibacterial properties using previously employed procedures.^[28] The prepared compounds were evaluated against two Gram-positive (*Staphylococcus aureus* [A] and *Klebsiella pneumonia* [B]) and two Gram-negative (*Escherichia coli* [C] and *Bacillus staphylococcus* [D]) bacterial strains. Antibacterial activities were tested against the four pathogenic bacterial species by adopting a disc diffusion bioassay method.^[29] Nutrient broth medium was prepared and 2% agar was added to it before it was autoclaved. The corresponding bacterial culture was revived from -80°C stock after overnight growth. Sterilized discs were soaked with 100 μl of sample solution and placed on plates, then the resulting culture was incubated at 37°C . The streptomycin and ampicillin were used as standard antibacterial agents in the same concentration (2 mg/ml) and DMSO solvent (as control) was also used. After overnight incubation, the zone of inhibition was measured in millimeters.

Antifungal bioassay

The antifungal activity of the synthesized compounds was tested against two fungal strains (*Aspergillus niger* [E] and *Aspergillus flavous* [F]) according to the recommended disc diffusion procedure.^[30] For antifungal bioassay, fungal cultures were revived in potato dextrose medium. Sterilized medium was transferred into Petri dishes, allowed to cool at room temperature, and then

sample was inoculated on discs. The medium was placed in an incubator for 48 hr and after completion of the incubation the process zone of inhibition was measured. Fluconazole was used as the standard antifungal drug.

2.2.4 | Antioxidant bioassay

DPPH radical scavenging assay

The antioxidant activity of the newly reported compounds was studied using a previously reported method.^[31] A sample of 1.0 mg/ml was dissolved in 4.0 ml of pure methanol, then 1 ml of methanolic solution (1.0 mM) in 2,2-diphenyl-1-picrylhydrazine (DPPH) was added. The resulting mixture was kept for 30 min under ambient conditions before measuring the absorbance at 515 nm in a UV-Vis spectrophotometer. Butylated hydroxytoluene (BHT) was used as the reference standard to compare the sample results. Percentage inhibition of DPPH was calculated as follows:

$$\text{percentage of inhibition} = A - B/B \times 100$$

where A is the absorbance of the blank and B is the absorbance of the sample.

Total phenolic contents

Total phenolic contents were evaluated by adopting a previously reported method.^[32] A 0.1 ml sample of solution (1.0 mg/ml) was transferred to a test-tube and 2 ml of sodium carbonate (7.5%) was added. After vortexing, 1.0 ml of Follin-Ciactleu reagent (10%) was added and the volume was made up to 10 ml with distilled water. The resulting mixture was allowed to stand for 30 min and then the absorbance was measured at 760 nm using a UV-Vis spectrophotometer. Gallic acid was used as the standard in this procedure. Measurements were made for each compound in triplicate.

Reducing power

The reducing power for all the synthesized products was evaluated using a previously reported method.^[33] A sample solution of 2.4 ml of 1.0 mg/ml sodium phosphate buffer (2 M, pH 6.6) and 5.0 ml of potassium ferricyanide (1%) were added in sequence to incubate the resulting mixture for 30 min at 50°C followed by the addition of 5.0 ml of trichloroacetic acid (10%). Centrifugation was done at 10,000 $\times\text{g}$ for almost 10 min. Then 5.0 ml of a solution of the supernatant layer was separated to add the 1.0 ml of 1.0% ferric chloride and the absorbance recorded at 700 nm using a UV-Vis spectrophotometer. To compare the results of the samples, a reference standard solution of BHT was prepared. All the

measurements were made in triplicate and the results were averaged.

Enzyme inhibition studies

An enzyme inhibition procedure was performed by spectrophotometry.^[34] Protease, amylase, acetylcholine esterase (AChE), and butyrylcholinesterase (BChE) were used as substrates. A mixture containing 0.5 ml of Tris buffer (pH 7.8), 50 μ l of 5,5-dithiobis-(2-nitrobenzoic acid), 100 μ l (5 mg/ml) of test compound solution, and 100 μ l of the specific enzyme was incubated at 37°C for 20 min. The reaction was initiated by the addition of 50 μ l of substrate. The sample was removed from the incubator and its activity measured using a UV-Vis spectrophotometer at 412 nm.

The percentage of enzyme inhibition was calculated as:

$$\text{percentage of inhibition} = K - L / L \times 100$$

where K is the absorbance of the blank and L is the absorbance of the sample.

3 | RESULTS AND DISCUSSION

Novel sulfonamide-derived Schiff bases L^1 and L^2 were air and moisture stable compounds with brick red color. Ligands were in crystalline form and melted at 209–226°C. All new sulfonamide-derived compounds were only soluble in ethanol, methanol, dioxane, N,N -dimethylformamide (DMF), acetonitrile, and DMSO. The ligands were coordinated with transition metals [VO(IV), Fe(II), Co(II), Ni(II), Cu(II), and Zn(II)] to prepare their metal complexes (Scheme 1) in a stoichiometric ratio of moles of 1:2 (metal:ligand). All the synthesized metal complexes were intensely colored and microcrystalline in nature. Cobalt, iron, nickel, and zinc were used as their chloride salts while vanadium and copper were used as their sulfates. Ligands and their coordination complexes **1–12** were characterized by their crystal, elemental, physical, spectral, and computational data. The physical properties of all the compounds are given in Table 1. The spectral and analytical data verified the composition and structures of the products.

TABLE 1 Physical and analytical measurements for complexes **1–12**

Complex	Formula	MW (g/mole) (yield %)	Color (MP, °C)	Elemental composition (%) found (calculated)			
				C	N	H	M
1	VO(L^1) ₂ (C ₂₈ H ₂₆ N ₄ O ₉ S ₂ V)	677.60 (71)	Light brown (281–283)	49.63 (48.89)	8.27 (8.32)	3.87 (3.12)	7.52 (7.34)
2	Fe(L^1) ₂ (H ₂ O) ₂ (C ₂₈ H ₃₀ FeN ₄ O ₁₀ S ₂)	702.53 (74)	Faded green (279–281)	47.87 (47.49)	7.97 (8.27)	4.30 (4.21)	7.95 (8.21)
3	Co(L^1) ₂ (H ₂ O) ₂ (C ₂₈ H ₃₀ CoN ₄ O ₁₀ S ₂)	705.62 (67)	Light orange (273–275)	47.66 (47.81)	7.94 (8.11)	4.29 (3.81)	8.35 (8.29)
4	Ni(L^1) ₂ (H ₂ O) ₂ (C ₂₈ H ₃₀ N ₄ NiO ₁₀ S ₂)	705.38 (65)	Green (261–263)	49.68 (48.97)	8.25 (8.21)	3.71 (3.11)	7.61 (8.21)
5	Cu(L^1) ₂ (H ₂ O) ₂ (C ₂₈ H ₃₀ CuN ₄ O ₁₀ S ₂)	710.24 (78)	Dark green (268–270)	47.35 (48.41)	7.89 (7.13)	4.26 (4.53)	8.95 (9.32)
6	Zn(L^1) ₂ (H ₂ O) ₂ (C ₂₈ H ₃₀ N ₄ O ₁₀ S ₂ Zn)	712.10 (61)	Off-white (293–295)	47.23 (47.19)	7.87 (8.10)	4.25 (4.29)	9.19 (9.65)
7	VO(L^2) ₂ (C ₃₆ H ₃₂ N ₆ O ₁₁ S ₂ V)	839.00 (81)	Light green (282–284)	51.24 (51.31)	9.96 (9.87)	4.30 (4.24)	6.04 (6.45)
8	Fe(L^2) ₂ (H ₂ O) ₂ (C ₃₆ H ₃₆ FeN ₆ O ₁₂ S ₂)	864.68 (73)	Yellow green (279–281)	49.77 (48.99)	9.67 (9.42)	4.64 (4.54)	7.38 (7.43)
9	Co(L^2) ₂ (H ₂ O) ₂ (C ₃₆ H ₃₆ CoN ₆ O ₁₂ S ₂)	867.77 (69)	Light orange (273–276)	49.60 (48.89)	9.64 (9.29)	4.62 (4.56)	6.76 (6.29)
10	(Ni(L^2) ₂ (H ₂ O) ₂ (C ₂₈ H ₃₀ N ₄ NiO ₁₀ S ₂)	705.38 (65)	Green (261–263)	49.61 (49.36)	9.64 (9.87)	4.63 (5.21)	6.73 (6.32)
11	(Cu(L^2) ₂ (H ₂ O) ₂ (C ₃₆ H ₃₆ CuN ₆ O ₁₂ S ₂)	836.35 (76)	Green (268–272)	49.34 (49.19)	9.5 (9.33)	4.6 (4.42)	7.25 (6.89)
12	(Zn(L^2) ₂ (H ₂ O) ₂ (C ₃₆ H ₃₆ ZnN ₆ O ₁₂ S ₂)	838.22 (64)	Off white (300 +)	49.46 (49.11)	9.61 (8.98)	4.59 (4.32)	7.4 (7.21)

Note. MP, melting point; MW, molecular weight.

3.1 | FT-IR spectra

The significant Fourier transform infrared (FT-IR) bands for the ligands and their transition metal complexes are given in the experimental section as well as in Table 2, and FT-IR spectra are shown in Supporting Information Figures S1–S8. Sulfonamide ligands have many donor sites: C=N, C–O, S–N, C–S, N–H, and SO₂. In the FT-IR spectra of the ligands, the sulfonamide NH₂ group and the aldehyde C=O group disappeared and a new band for azomethine (HC=N) linkage was observed at 1604–1607 cm⁻¹.^[35] Both ligands displayed a broad band at 3309 cm⁻¹ for ν (OH). The appearance of two bands at 1345 and 1110 cm⁻¹ were assigned to the ν_{asymm} (SO₂) and ν_{symm} (SO₂) groups, respectively. Furthermore, the ligands also displayed characteristic bands at 1386 and 1282 cm⁻¹ due to C–O and C=C linkages, respectively.^[36] The bonding of azomethine with metal ions was evidenced via a shift to a lower frequency at 12–20 cm⁻¹ (1587–1592 cm⁻¹) in all metal complexes.^[37] The disappearance of the ν (OH) band at 3309 cm⁻¹ in both ligands and the presence of new bands at 1385–1395 cm⁻¹ in all metal complexes due to ν (C–O) vibrations indicated the deprotonation of the OH group found in the ligand and complexation of the phenolic-O group of the ligand with the metal atoms.^[38] All the metal complexes possessed new broad peaks at 3195–3205 cm⁻¹ which were attributed to water molecules.^[8] The bands for ν (SO₂) and ν (SO₂) for the ligands at around 1345 and 1110 cm⁻¹ remained unchanged, indicating their noninvolvement during coordination. The emergence of new bands in the spectra of compounds **1** and **7** in the 978–982 cm⁻¹ region

confirmed the incorporation of the V=O group in the prepared coordination compounds.^[30] All these indications confirm the coordination of the transition metal ions with the synthesized Schiff bases.

3.2 | ¹H NMR spectra

The ¹H NMR spectra for the ligands were determined in DMSO-d₆. The possible ¹H NMR spectral assignments are given in the experimental section. The ¹H NMR spectra of both ligands exhibited the singlet peak of azomethine at 8.96 ppm^[39] while the protons of the hydroxyl groups had singlet peaks at 12.51–12.72 ppm. The pyrimidine C₅–H protons of the ligands had peaks at 7.54–7.58 ppm as multiplets while their C₆–H protons had peaks at 7.88–7.94 ppm. The methoxy protons of both ligands appeared as singlets at 2.92–3.32 ppm. The –SO₂NH– protons in **L**¹ had a singlet peak at 3.85 ppm (Supporting Information Figures S9 and S10). All the protons were found in their expected regions, supporting the binding mode evidence through their IR spectral studies.

3.3 | ¹³C NMR spectra

The ¹³C NMR spectra for the ligands were also obtained in DMSO-d₆. The possible spectral assignments for both ligands are given in the experimental section. The carbon atoms were found to be in their expected region, supporting the binding possibilities evidenced by the FT-IR and ¹H NMR spectral data. The carbon of azomethine

TABLE 2 Conductance, magnetic moments, UV–Vis, and FT-IR spectral data for complexes **1–12**

Complex	Ω_M ($\Omega^{-1} \text{ cm}^2 \text{ mol}^{-1}$)	μ_{eff} , BM	λ_{max} (cm ⁻¹)	FT-IR (cm ⁻¹)
1	12.1	2.30	13450, 18160, 26420	1587 (HC=N), 1388 (C–O), 978 (V=O), 956 (S–N), 841 (C–S)
2	12.4	3.10	10160, 10354	1592 (HC=N), 1395 (C–O), 956 (S–N), 841 (C–S)
3	17.2	1.40	7572, 17440, 29123	1592 (HC=N), 1390 (C–O), 956 (S–N), 841 (C–S)
4	12.5	2.10	10116, 15850, 24875	1590 (HC=N), 1393 (C–O), 956 (S–N), 841 (C–S)
5	12.0	2.30	14995, 19441, 30367	1587 (HC=N), 1386 (C–O), 956 (S–N), 840 (C–S)
6	21.0	Dia.	29405	1592 (HC=N), 1395 (C–O), 958 (S–N), 841 (C–S)
7	12.5	2.30	13435, 18269, 26427	1587 (HC=N), 1388 (C–O), 956 (S–N), 841 (C–S), 982 (V=O)
8	13.2	4.10	10197, 10287	1592 (HC=N), 1385 (C–O), 955 (S–N), 841 (C–S)
9	12.4	2.40	7520, 17950, 29321	1592 (HC=N), 1389 (C–O), 956 (S–N), 841 (C–S)
10	16.2	1.87	9889, 15788, 25003	1583 (HC=N), 1392 (C–O), 959 (S–N), 841 (C–S)
11	12.5	2.43	15246, 19322, 30335	1587 (HC=N), 1388 (C–O), 958 (S–N), 841 (C–S)
12	19.0	Dia.	29971	1589 (HC=N), 1395 (C–O), 956 (S–N), 841 (C–S)

Note. Dia, Diamagnetic.

($-\text{HC}=\text{N}$)^[40] in both ligands was observed at 158.1–160.9 ppm. The carbon C₂ of the pyrimidine moiety showed a very minor shift (150.8 to 150.9 ppm), probably due to the absence of an electron-withdrawing group at C₅, C₃, and C₄. However, the C₅ of the same moiety experienced a downwards shift, that is, 123.6 ppm to 115.0 ppm, attributed to the conjugation of the azomethine group. The C₁ of the methoxyphenyl group of ligand **L**¹ showed a downward shift from 121.6 ppm to 119.37 ppm owing to the presence of the hydroxyl group at the C₂ position. The peak at 56.10 ppm indicated the presence of methoxy groups (Supporting Information Figures **S11** and **S12**).

3.4 | Mass spectra

The mass spectra for the main fragments of ligand **L**¹ along with its molecular ion peaks are given in Supporting Information Figure **S13**. Mass spectral studies indicated that the ligands and their corresponding complexes are coherent with their designs. The molecular mass of **L**¹ was observed to be 306.0 (C₁₄H₁₄N₂O₄S) and the most stable fragment^[41] was found at $m/z = 226$ for the [C₁₄H₁₂NO₂]⁺ fragment. Other peaks in order of increasing abundance were 123 (2.31%), 136.14 (11.45%), 183.08 (18.22%), 226 (100%), 252 (30.12%), and 275 (21.44%). The mass spectra of the metal complexes were also consistent with the computed masses of their intended formulae. The molecular mass of the vanadyl complex (C₂₈H₂₆N₄O₉S₂V) was observed to be m/z 677 (calcd 677.6), with the most stable fragment, C₂₈H₂₄N₃O₇SV, at m/z 597.5 along with other mass fragments in increasing abundances of 486.08 (12%), 517 (51%), 662.22 (23%), and 597.51 (100%) (Supporting Information Figure **S14**). The molecular mass of the copper complex (C₂₈H₃₀CuN₄O₁₀S₂) was observed at m/z 710 (calcd 710.1), with the C₁₃H₁₂CuN₄O₆S₂⁻ fragment the most stable one (base peak) at m/z 447.9 along with other fragmental peaks with percentages of 305 (34%), 306 (51%), 662.22 (23%), 399 (71%), and 446 (100%) (Supporting Information Figure **S15**). The molecular ionic peak [M + 1]⁺ for ligand **L**² was found at m/z 387, which agrees with the theoretically calculated m/z value of 387 (Supporting Information Figure **S16**). The base peak for the most stable fragment was confirmed at m/z 226.25, with other fragments at 361.37 (2.31%), 259.28 (21.32%), 226.25 (100%), 182.19 (8.4%), and 150 (7.89%). The vanadyl complex had a base peak of m/z at 254.08 and there were other fragments at 388.17 (68%), 517 (12%), 295 (64%), and 484 (69%) (Supporting Information Figure **S17**). The zinc complex had a base peak of m/z 518.17 (100%) with

other fragmental peaks at 425 (60%), 452.08 (78%), 502 (59%), and 721 (82%) (Supporting Information Figure **S18**). The base peaks for all the metal complexes were found to have different m/z concerning their metal complexes.^[41] The features of the sulfonamide Schiff bases determined by the mass spectra strongly confirmed that the synthesis of the ligands produced their proposed structures and bonding patterns.

3.5 | Molar conductivity measurements

The molar conductivities of 1×10^{-3} M solutions of complexes **1–12** were measured in DMF at room temperature and are listed in Table 2. All the values for these metal complexes fell in the range $12\text{--}19 \Omega^{-1}\cdot\text{cm}^2\cdot\text{mol}^{-1}$, indicating that these chelates are nonelectrolytic^[42] in their nature and ruling out the presence of any counterions in the proposed structures.^[43]

3.6 | Magnetic susceptibilities

Magnetic susceptibilities are a very useful technique for determining the stereochemistry of metal ions in complexes.^[44] They also provide essential information about the number of unpaired electrons, leading to the determination of the geometry of complexes.^[45] The magnetic moment readings were the range 4.67–4.79 BM, specifying their paramagnetic nature owing to the presence of three unpaired electrons, which also implies octahedral geometry for Co(II) complexes.^[46] The magnetic moments for Ni(II) complexes were found in the 3.13–3.22 BM range, confirming the partial covalent character for metal–ligand bonds and also the octahedral geometry around Ni(II) foci.^[47] The experiential magnetic moment values of Cu(II) complexes were found in the 1.41–1.72 BM range, suggesting octahedral geometry for them.^[48] The magnetic moment for Zn(II) complexes was found to be zero, confirming its diamagnetic nature.^[49]

3.7 | Single crystal X-ray analysis

The synthesized Schiff base of sulfonamide (**L**¹) was analyzed by SC-XRD.^[50] Crystallographic data are listed in Table 3 and information on hydrogen bonds with co-crystals is given in Table 3. A view of the structure of **L**¹ showing the atom labeling scheme is shown in Figure 1. Displacement ellipsoids were drawn at the 50% probability level. Crystal structure data were deposited at the Cambridge Crystallographic Data Centre.

TABLE 3 Experimental details for crystal of ligand **L**¹

Cambridge Crystallographic Data Centre (CCDC) number		1903654
Chemical formula	C ₁₄ H ₁₄ N ₂ O ₄ S	
<i>M_r</i>	306.33	
Crystal system, space group	Monoclinic, <i>P</i> ₂ ₁ / <i>c</i>	
Temperature (K)	296	
<i>a</i> , <i>b</i> , <i>c</i> (Å)	9.1828 (11), 10.9199 (12), 14.621 (2)	
β (°)	102.860 (6)	
<i>V</i> (Å ³)	1429.4 (3)	
<i>Z</i>	4	
Radiation type	Mo <i>K</i> α	
μ (mm ⁻¹)	0.24	
Crystal size (mm)	0.42 × 0.32 × 0.28	
Data collection		
Diffractometer	Bruker Kappa APEXII CCD	
Absorption correction	Multi-scan (SADABS; Bruker, 2005)	
<i>T</i> _{min} , <i>T</i> _{max}	0.880, 0.955	
No. of measured, independent, and observed <i>I</i> > 2σ(<i>I</i>) reflections	8995, 3269, 2570	
<i>R</i> _{int}	0.044	
(sin θ/λ) _{max} (Å ⁻¹)	0.651	
Refinement		
<i>R</i> [<i>F</i> ² > 2σ(<i>F</i> ²)], <i>wR</i> (<i>F</i> ²), <i>S</i>	0.046, 0.129, 1.04	
No. of reflections	3269	
No. of parameters	200	
Hydrogen atom treatment	Hydrogen atoms treated by a mixture of independent and constrained refinement	
Δ _{max} , Δ _{min} (e Å ⁻³)	0.30, -0.36	

3.8 | Structural optimization

Density functional theory (DFT) at the B3LYP level of approximation with 6-311+G(d,p) as the basis set was used to obtain the structural parameters of **L**¹. The DFT-based optimized structure with the experimental structural parameters of the entitled compound is shown in Supporting Information Table S1. The values of the structural parameters that were obtained in same amplitudes of DFT and SC-XRD were R(C13–C14), N(1)–C(9)–C(10) and C(2)–C(1)–C(8) (Supporting Information Table S1). The C–C bond lengths in the benzene ring were found to be 1.413, 1.389, 1.378, 1.388, 1.394, and 1.392 Å by DFT,

corresponding closely with the values of 1.401, 1.376, 1.376, 1.379, 1.384, and 1.377 Å found by SC-XRD. The related value obtained with a bond length of carbonyl group C=O in **L**¹ was determined to be 1.337 Å by DFT, which is in good agreement with the SC-XRD value of 1.35 Å. The C(12)–S(1) and S(1)–N(2) bond lengths in **L**¹ were determined to be 1.793 and 1.696 Å by DFT and 1.766 and 1.603 Å by SC-XRD. The S(1) = O (4) and S(1) = O (5) bond lengths were determined to be 1.461 and 1.461 Å by DFT, and 1.427 and 1.433 Å by SC-XRD. The N(1)–C(8) and N(1)–C(9) bond lengths were determined to be 1.29 and 1.404 Å by DFT, which agree with the values estimated by SC-XRD of 1.27 and 1.422 Å, respectively (Supporting Information Table S1 and Figure 2). DFT gave values of 119.5°, 122.6°, 125.3°, 120.4°, 119.6°, 120.5° and 119.3° for the bond angles S(1)–C(12)–C(11), O(1)–C(2)–C(1), O(2)–C(3)–C(4), C(1)–C(6)–C(5), C(2)–C(3)–C(4), C(9)–C(10)–C(11), and C(10)–C(11)–C(12), respectively. The values for these angles obtained by SC-XRD were 119.4°, 122.4°, 125.6°, 120.3°, 119.7°, 120.4°, and 119.4°, respectively (Supporting Information Table S1 and Figure 3). In summary, DFT-based parameters for the chemical structure were found to agree with SC-XRD data.

3.9 | Hirshfeld surface analysis

Hirshfeld surfaces at two configurational modes for ligand **L**¹ are shown in a Hirshfeld surface plot (Figure 4) in which red indicates the strongest interactions, intermediate interactions are shown in white, and almost negligible intermolecular interactions are shown in blue. Possible hydrogen bond parameters are given in Table 4. Interactions at the molecular level were also computed using two-dimensional plots at a two-dimensional level, having the decomposition quantifying the individual contributions for each intermolecular interaction included in the structure. In the crystal packing for **L**¹, the O[⋯]H contacts appeared to be the major contributor (33.3%). The percentages of intermolecular contributions for different interatomic contacts to the Hirshfeld surface of molecule are shown in Table 5. It can be seen that O[⋯]H, H[⋯]H, C[⋯]H, and N[⋯]H contacts made large contributions (Figure 5). In order to classify the hydrogen-bonded donor and acceptor groups of **L**¹, the electrostatically mapped Hirshfeld surfaces were computed using TONTO software^[51] at standard settings of STO-3G basis set at Hartree–Fock theory.^[52] The blue and red shading indicates the positive and negative electrostatic potentials for the two surfaces (Figure 6). The unprotonated oxygen atoms of the hydroxyl group, the ether group, and the unprotonated nitrogen atom act as hydrogen bond acceptors.

FIGURE 1 The structure of L^1 showing the atom labeling scheme. Displacement ellipsoids are drawn at the 50% probability level

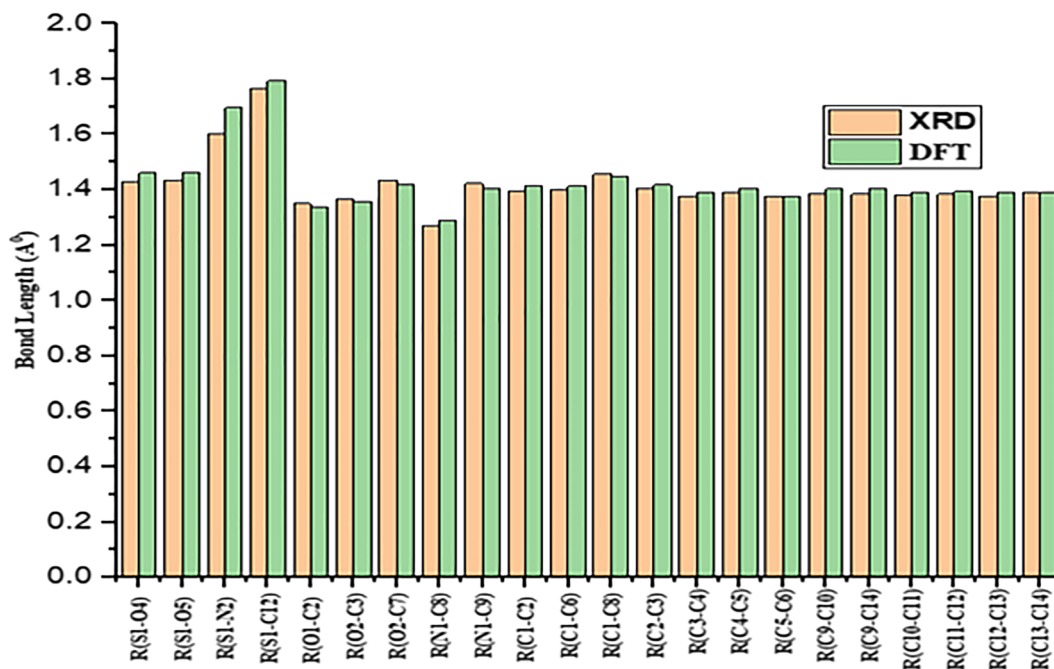
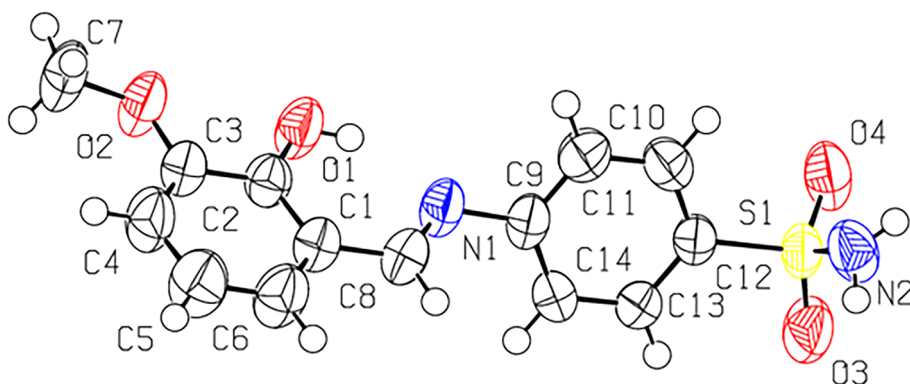


FIGURE 2 Comparative bond lengths at SC-XRD and DFT levels for L^1

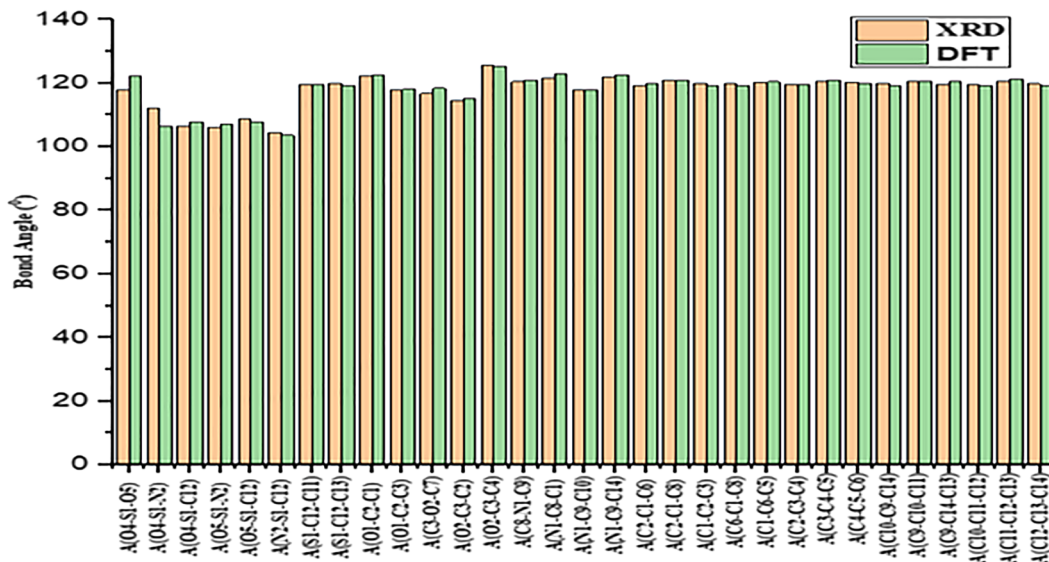


FIGURE 3 Comparative of bond angles of SC-XRD and DFT for L^1

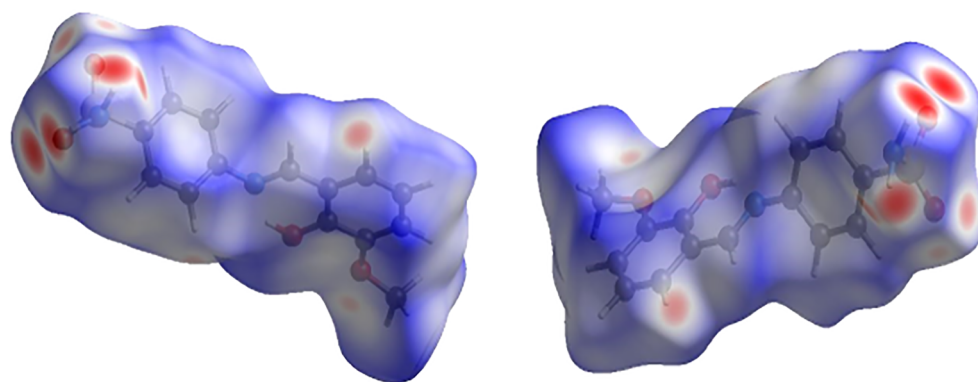


FIGURE 4 Hirshfeld surfaces mapped at two views over d_{norm} for L^1 ranging from -0.4855 to 1.4354 a.u. (1 a.u. of electron density = $6.748 \text{ e}\text{\AA}^{-3}$)

TABLE 4 Selected hydrogen-bond parameters of ligand L^1

D-H...A	D-H (Å)	H...A (Å)	D...A (Å)	D-H...A (°)
O1-H1...N1	0.82	1.88	2.5997 (19)	146.3
N2-H2A...O4	0.80 (3)	2.18 (3)	2.984 (2)	175 (3)
N2-H2B...O1	0.84 (3)	2.20 (3)	2.976 (2)	153 (3)
N2-H2B...O2	0.84 (3)	2.42 (3)	3.086 (2)	137 (3)
C10-H10...O2	0.93	2.61	3.480 (3)	155.8
C14-H14...O3	0.93	2.60	3.468 (3)	155.4

Note. A, acceptor; D, donor.

TABLE 5 Contributions (%) of interatomic contacts to the Hirshfeld surface for L^1

Contact	Contribution (%)
O...H / H...O	33.3
H...H	32.1
H...C / C...H	30.2
H...N / N...H	2.4
O...C / C...O	1.2
N...N	0.4
C...C	0.2
N...C / C...N	0.1

3.10 | NBO analysis

Natural bonding orbital (NBO) analysis was performed using the Gaussian 09 program with DFT and transfigured the molecular orbitals into a new molecular orbitals set that which could be carefully trussed to chemical bonding principles. This technique involved the successful conversion of nonorthogonal atomic orbitals to units of natural atomic orbitals, natural hybrid orbitals, and NBOs. The localized basis set described the wave capabilities within the maximum economic approach, as electron density and different characters are defined via the slightest amount of filled NBOs, which delineated the hypothetical, strictly localized Lewis shape which might

be used as the degree of delocalization. The second-order perturbation interaction energy ($E^{(2)}$) can be used to explain the noncovalent bonding quantitatively as well as antibonding charge-transfer interactions.^[53] The stabilization energy equation as per the second-order perturbation theory is:

$$E^{(2)} = q_i \frac{(F_{ij})^2}{\epsilon_j - \epsilon_i} \quad (1)$$

where q_i denotes the occupancy of the donor orbital, s_j and s_i are the off-diagonal NBO Fock matrix elements, $E^{(2)}$ is the stabilization energy, and F_{ij} is the diagonal energy. (The better degree for the bonding and antibonding orbitals interaction was apparent from the degree of perturbation stabilization energy ($E^{(2)}$).

The NBO numbering scheme for ligand L^1 is given in Figure 7. The Ligand, L^1 contained $\sigma \rightarrow \sigma^*$, $\pi \rightarrow \pi^*$, lone pair (LP) $\rightarrow \sigma^*$, and LP $\rightarrow \pi^*$ transitions, as can be seen in Supporting Information Table S2. Here we discuss some hyperconjugative interactions as representative values. The maximum conceivable electronic transitions were found to be LP(O2) $\rightarrow \pi^*(\text{C11-C12})$ and LP(O4) $\rightarrow \pi^*(\text{C13-C14})$ with stabilization energy values of 37.65 and 30.39 kcal/mol, respectively. Moreover, some ($\pi \rightarrow \pi^*$) transitions were seen, namely, $\pi(\text{C26-C34}) \rightarrow \pi^*(\text{C31-C32})$, $\pi(\text{C11-C12}) \rightarrow \pi^*(\text{N7-C24})$, $\pi(\text{C27-C29}) \rightarrow \pi^*(\text{C26-C34})$, $\pi(\text{C31-C32}) \rightarrow \pi^*(\text{C27-C29})$, $\pi(\text{C11-}$

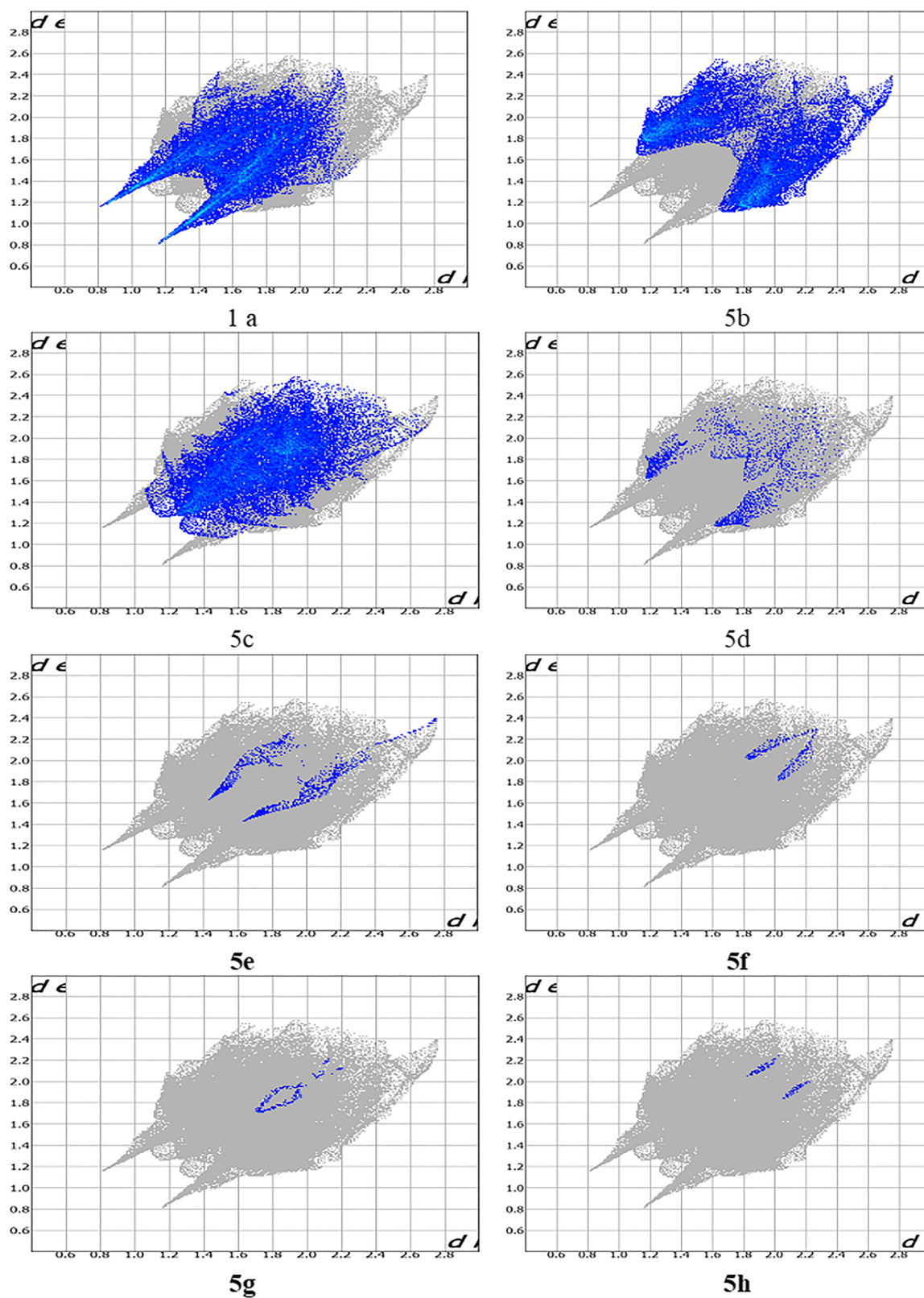


FIGURE 5 Fingerprint plot contacts of (a) O...H, (b) H...H, (c) C...H, (d) N...H, (e) C...O, (f) N...N, (g) C...C, and (h) C...N

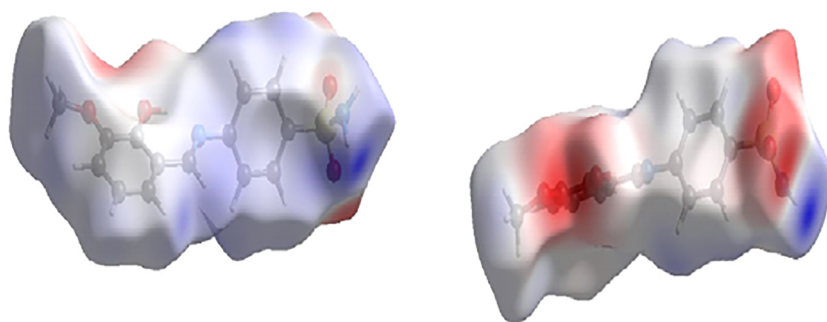


FIGURE 6 Electrostatically mapped Hirshfeld surfaces of L^1 in the range -0.1111 to 0.1257 a.u. using the STO-3G basis set at the Hartree-Fock level. The hydrogen bonding interactions for the acceptor/donor atoms of $O-H \cdots O$ and $N-H \cdots O$ are shown as blue and red shading around the atoms, depicting positive and negative potentials, respectively

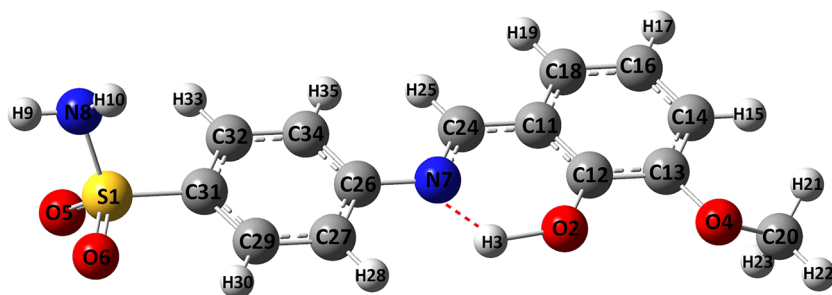


FIGURE 7 NBO numbering scheme for L^1

$C12 \rightarrow \pi^*(C16-C18)$, $\pi(C13-C14) \rightarrow \pi^*(C11-C12)$, $\pi(C16-C18) \rightarrow \pi^*(C13-C14)$, $\pi(C13-C14) \rightarrow \pi^*(C16-C18)$, and $\pi(N7-C24) \rightarrow \pi^*(C26-C34)$ with stabilization energies of 25.18, 22.66, 21.96, 20.94, 19.74, 18.86, 18.24, 17.59, and 10.70 kcal/mol, respectively, which revealed the degree of conjugation in L^1 . The intramolecular charge transfer, hyperconjugative interactions, and expanded conjugation were the main reasons for the stability of L^1 . These interactions were found to be in excellent agreement with the SC-XRD data.

3.11 | Mulliken atomic charge analysis

In quantum chemical analysis, Mulliken atomic charge investigation of any molecular system has a vital role to play in obtaining the dipole moment, electronic properties, and molecular polarizability of the chemical

system.^[54] The Mulliken population examination of L^1 was found to use the B3LYP level with a 6-311+G(d,p) basis set. The Mulliken charge distribution of L^1 is shown in Figure 8. The charge dissemination of L^1 shows that all oxygen atoms linked with sulfur, nitrogen, and hydrogen atoms (S1, C12, and C13) are negatively charged, whereas the nitrogen atoms connected with oxygen atoms such as O5 and O6 are slightly positively charged. Moreover, the nitrogen atoms attached to hydrogen and carbon atoms adjacent to the nitrogen atoms are also positively charged. Some carbon atoms coupled with carbon and nitrogen atoms were found to have significant negative charges.

3.12 | FT-IR analysis

Ligand L^1 having 35 atoms involving nitrogen, oxygen and sulfur atoms contained 99 vibration modes having

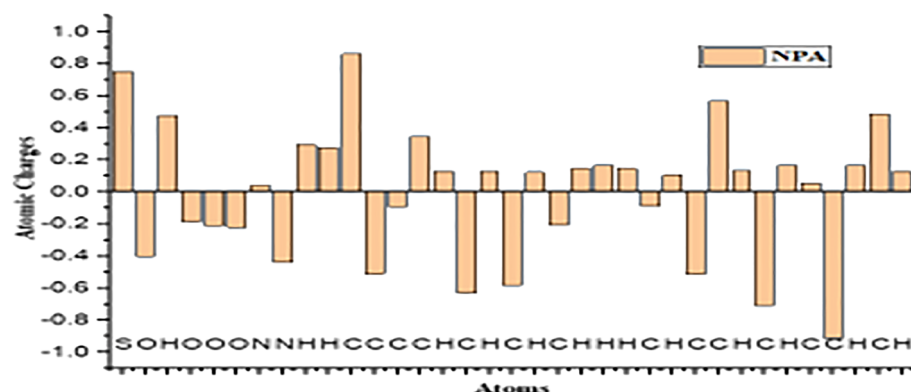


FIGURE 8 Mulliken charge distribution of L^1

point group symmetry of C₁. The FT-IR frequencies for **L**¹ are shown in Supporting Information Table S3. The stretching vibrational modes for the aromatic C–H were observed at 3000–3100 cm⁻¹ with the combinational (overtone) peaks owing out-of-plane bending vibrations seen at 2000–1660 cm⁻¹.^[55] The symmetric C–H modes for methyl and methoxy were seen at 2925–2985 cm⁻¹. The FT-IR stretching vibrations of aromatic C=C and C–C were seen at 1650–1400 cm⁻¹. These FT-IR stretching vibrations are shown in detail in Supporting Information Table S3. The significant functional groups are listed here in detail: *S=O vibrations* Stretching vibration bands for SO₂ were seen at 1130 and 1315 cm⁻¹ (DFT) and 1155 and 1262 cm⁻¹ (experimental).

NH₂ vibrations The modes for NH₂ were seen at 3512 and 3620 cm⁻¹ (DFT) and 3205 cm⁻¹ (experimental).

O–H vibrations The stretching vibration for O–H was seen at 3251 cm⁻¹ (DFT) and 3309 cm⁻¹ (experimental).

CH=N vibration The vibration for CH=N was seen at 1665 cm⁻¹ (DFT) and 1580 cm⁻¹ (experimental).

N–H vibrations The vibration for N–H was seen at 1337 cm⁻¹ (DFT) and 1312 cm⁻¹ (experimental).

The DFT-based vibrational modes were therefore found to be in agreement with the experimental ones (Supporting Information Table S3).

3.13 | UV–Vis spectra

Time-dependent density functional theory (TD-DFT) calculations in the gas phase were carried out at the B3LYP/6-311+G(d,p) level of approximation^[56] on the absorption spectra of **L**¹. The maximum absorption wavelength (λ_{max}), transition state, oscillator strength, and calculated transition energy values are shown in Supporting Information Table S4. **L**¹ displayed absorbance in the visible region and the highest calculated λ_{max} value was seen at 387 nm (Supporting Information Figure S19). Experimental UV–Vis spectra for the ligands and their complexes were done in DMF solvent. Oxovanadium(IV) complexes of both ligands showed typical bands at 13435–13450, 18160–18269, and 26420–26427 cm⁻¹ for B₂ → E_π, B₂ → B₁, and B₂ → A₁ transitions.^[30] The appearance of a band at 30131–30391 cm⁻¹ confirmed the metal → ligand charge transfer phenomenon. All the observed bands confirmed the square pyramidal geometry of both vanadium complexes.^[20] The Fe(II) complexes showed two typical electronic transitions at 10160–10197 and 10287–10354 cm⁻¹, implying 5T_{2g} and 5E_g transitions and confirming their octahedral symmetries. The Co(II) complexes showed two low energy absorption bands for to 4T_{1g}(F) → 4T_{2g}(F) and 4T_{1g}(F) → 4T_{1g}

(P) transitions,^[42] with ranges of 7520–7572 and 17950–17440 cm⁻¹ and a high energy band in the range of 29123–29321 cm⁻¹, proving their high-spin octahedral geometry. For the Ni(II) complexes, three absorption bands were seen^[29] at 9889–10116, 15788–15850, and 24875–25003 cm⁻¹ due to 3A_{2g}(F) → 3T_{2g}(F), 3A_{2g}(F) → 3T_{1g}(F), and 3T_{2g}(F) → 3T_{1g}(P) transitions. The spectra recorded for the Cu(II) complexes confirmed two bands at 14995–15246 and 19441–19322 cm⁻¹, attributed to 2B_{1g} → 2A_{1g} and 2B_{1g} → 2E_g transitions and confirming their octahedral geometry, along with a high-intensity band at 30335–30367 cm⁻¹ due to metal → ligand charge transfer.^[14] No characteristic d–d transition bands were recorded for the diamagnetic nature of the corresponding Zn(II) complexes. Only the strong band of high intensity was recorded at 29405–29971 cm⁻¹ due to metal → ligand charge transfer.^[20]

3.14 | FMO analysis

Frontier molecular orbitals (FMOs) such as the highest occupied molecular orbital (HOMO) and lowest unoccupied molecular orbital (LUMO) give useful insights into the estimation of chemical and molecular stability.^[57] Furthermore, the energy difference ($E_{\text{LUMO}} - E_{\text{HOMO}}$) between the LUMO and HOMO was used to estimate the most important features of the studied molecules, including chemical reactivity, optical polarizability, chemical softness, and chemical hardness.^[58] The energies of the FMOs were computed using the B3LYP/6-31+G(d,p) level of theory and the results are shown in Table 6. Three substantial FMO pairs, HOMO → LUMO, HOMO-1 → LUMO+1, and HOMO-2 → LUMO+2 were analyzed (Figure 9). The intramolecular charge transfer was confirmed by the FMO phenomenon as can be seen in the electronic transition between HOMO and LUMO in Figure 9. It is conspicuous to know that HOMO represents bonding character while LUMO reflects antibonding character. The energy gaps for HOMO → LUMO, HOMO-1 → LUMO+1, and HOMO-2 → LUMO+2 were observed to be 0.138, 0.208, and 0.241 Hartree energy (E_{h}), respectively. The energy gap is thought to be inversely related to reactivity and directly

TABLE 6 E_{HOMO} , E_{LUMO} , and the energy band gap ($E_{\text{LUMO}} - E_{\text{HOMO}}$) for the ligands

Transitions	E_{HOMO}	E_{LUMO}	Band gap
HOMO → LUMO	-0.227	-0.089	0.138
HOMO-1 → LUMO+1	-0.249	-0.041	0.208
HOMO-2 → LUMO+2	-0.277	-0.036	0.241

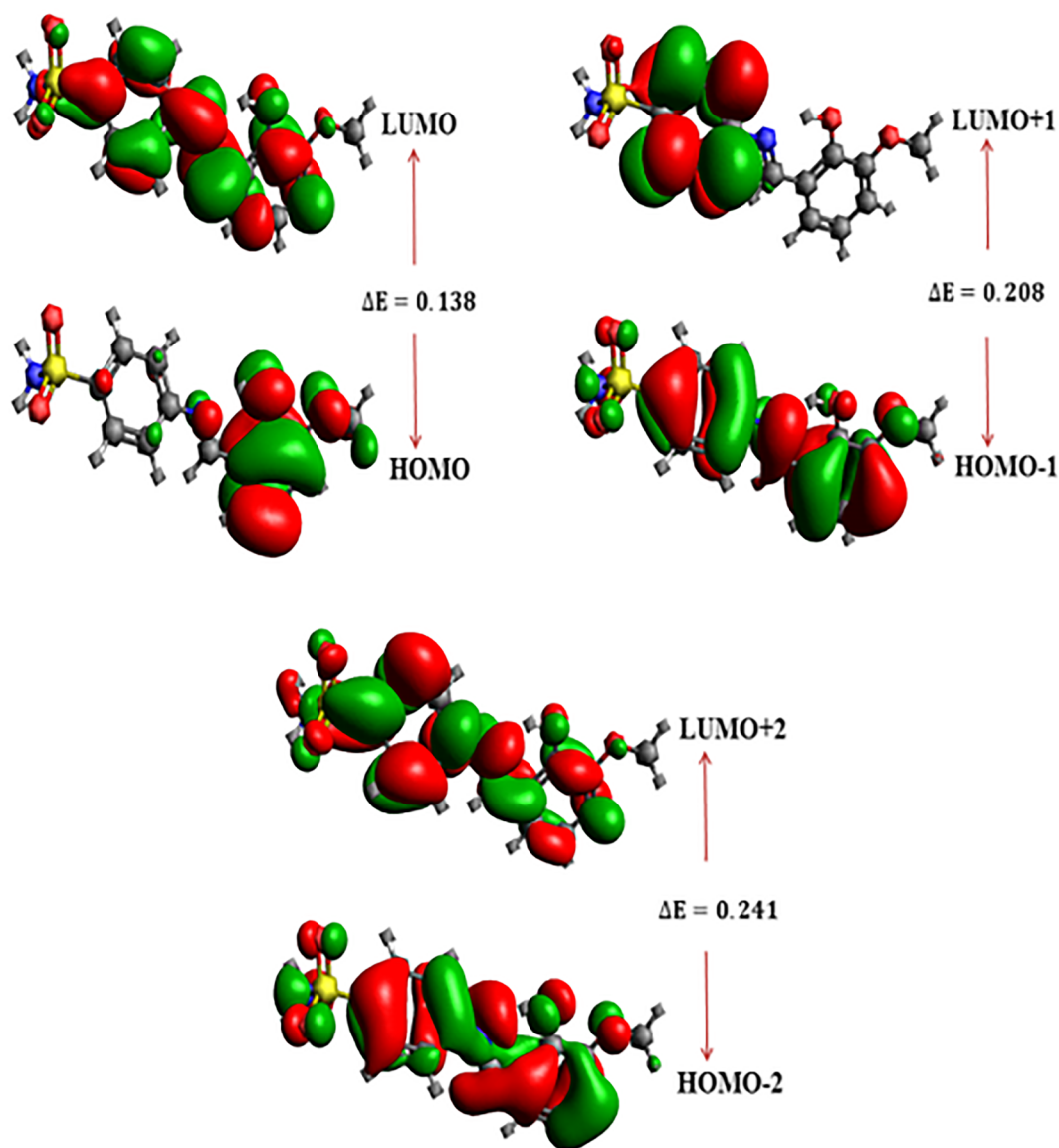


FIGURE 9 HOMOs and LUMOs of L^1

associated with the stability/strength of the species. Molecules with a small gap ($E_{\text{LUMO}} - E_{\text{HOMO}}$) are soft, chemically unstable, and reactive molecules. On the contrary, chemically hard, stable, and less reactive molecules have larger $E_{\text{LUMO}} - E_{\text{HOMO}}$ gap values.

The global reactivity descriptors electronegativity (E_A), chemical potential (I), global hardness (η), global softness (S), and electrophilicity index (ω) were obtained using E_{LUMO} and E_{HOMO} and equations S1–S5 in the Supporting Information. The results are shown in Supporting Information Table S5. The ionization potential and electron affinity values were obtained to be 0.227 and 0.089 (at HOMO \rightarrow LUMO level), respectively. The ionization potential values were observed larger to some extent as compared to electron affinity values describing

the better electron-donating capability of the investigated molecule. The global hardness value was found to be 0.069 and the global softness value was 7.246377 (at HOMO \rightarrow LUMO level), which shows that the L^1 is less stable and more reactive. The ligand therefore had a strong tendency to form complexes with different metals (Figure 9).

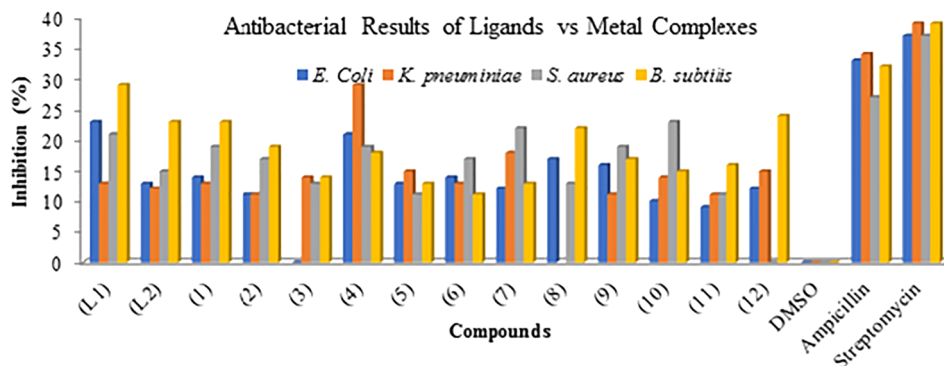
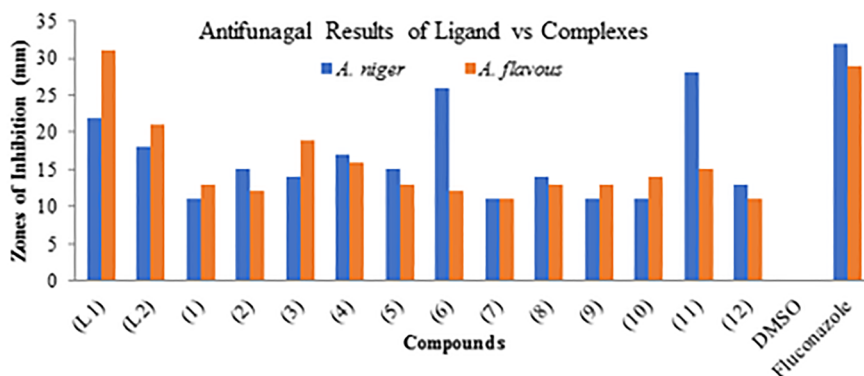
3.15 | NLO properties

The structural diversity of organic compounds gives the potential to be used in the fields of electronics, photonics, and nonlinear optics (NLO).^[59] The B3LYP level of theory with a 6-311+G(d,p) basis set was used to observe

TABLE 7 Antibacterial and antifungal results for ligands L^1 and L^2 and complexes 1–12

Complex	Bacterial strains				Fungal strains	
	A	B	C	D	E	B
L^1	23	13	21	29	22	31
L^2	13	12	15	23	26	12
1	14	13	19	23	–*	11
2	11	11	17	19	11	13
3	–*	14	13	14	15	12
4	18	29	19	18	14	19
5	13	15	11	13	17	16
6	14	13	17	11	15	13
7	12	18	22	13	11	11
8	16	–*	13	22	14	13
9	16	11	19	17	11	13
10	10	14	23	15	11	14
11	9	11	11	16	28	15
12	12	15	–*	24	13	11
DMSO	–*	–*	–*	–*		
Ampicillin	33	34	27	32		
Streptomycin	37	39	37	39		
Fluconazole					32	29

*Inactive. Note. A, *E. coli*; B, *K. pneumoniae*; C, *S. aureus*; D, *B. subtilis*; E, *A. niger*; F, *A. flavus*. DMSO, dimethyl sulfoxide.

FIGURE 10 Antibacterial activities of ligand vs. complexes**FIGURE 11** Antifungal activities of ligands vs. complexes

the NLO parameters for the B3LYP. The linear polarizability was determined using equation (2):

$$\langle a \rangle = 1/3(a_{xx} + a_{yy} + a_{zz}) \quad (2)$$

The first hyperpolarizability (β_{tot}) was determined using equation (3):

$$\beta_{tot} = [(\beta_{xxx} + \beta_{xyy} + \beta_{zzz})^2 + (\beta_{yyy} + \beta_{xxy} + \beta_{yzz})^2 + (\beta_{zzz} + \beta_{xxz} + \beta_{yyz})^2]^{1/2} \quad (3)$$

The first-order polarizabilities along the α_{xx} , α_{yy} , and α_{zz} directions were observed to be 402.175, 206.76, and 135.89 a.u., respectively, which resulted in an $\langle a \rangle$ value of 248.27 a.u. The second-order polarizability (β_{tot}) values along with their major contributing tensors, that is, β_{xxx} , β_{xxy} , β_{xyy} , β_{yyy} , β_{xxz} , β_{yyz} , β_{xzz} , β_{yzz} , β_{zzz} , and β_{tot} were observed to be -1422.11 , 243.78 , -30.694 , 348.579 , 83.222 , 46.098 , 91.483 , 89.007 , 96.029 , and 1538.919 a.u. Urea is a standard compound commonly used in the literature to compare dipole moments and first-order hyperpolarizability data. L^1 had a higher dipole moment than urea (1.3732 D).^[60] Similarly, the β_{tot} value of L^1 was found to be greater than that of urea ($\beta_{tot} = 43$ a.u.).

3.16 | Biological evaluation

3.16.1 | Antibacterial bioassay

All the synthesized products were examined *in vitro* for their antibacterial features against two Gram-positive (*S. aureus* and *B. subtilis*) and two Gram-negative (*E. coli* and *K. pneumoniae*) bacterial strains. The antibacterial activities of the Schiff base ligands and their transition

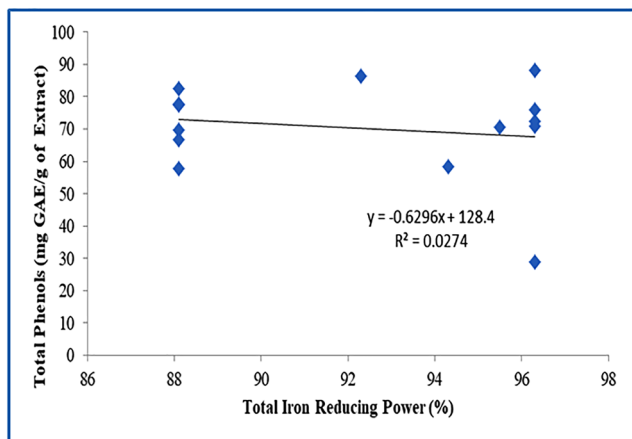
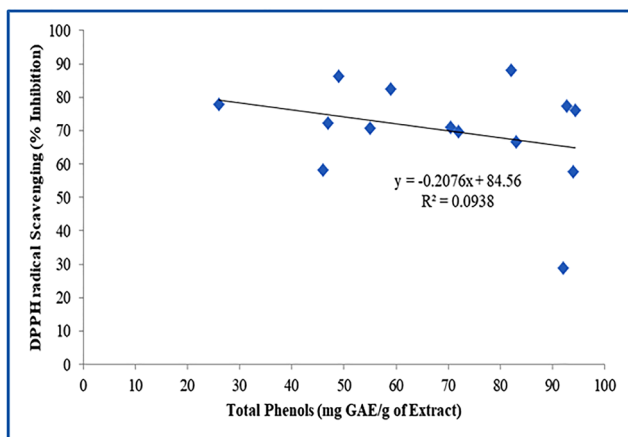
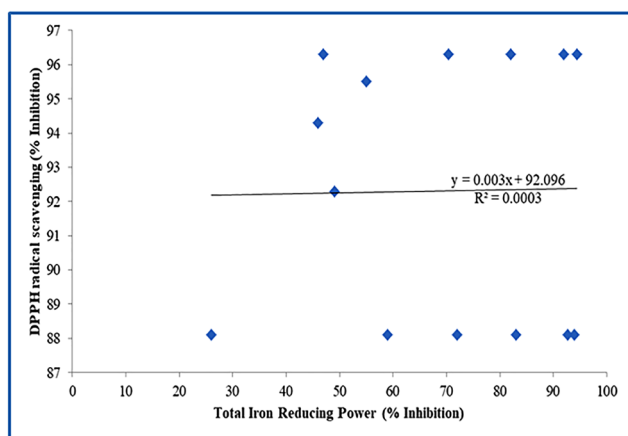


FIGURE 12 Correlational studies of antioxidant values

metal complexes were evaluated by comparing them with the two standard drugs streptomycin and ampicillin. The activities of each sample were recorded in millimeters (mm) as their zone of inhibition (Table 7). The data revealed that all the compounds had different inhibition degrees compared to tested bacterial strains concerning their growth not varying significantly from literature. Both the ligands exhibited moderate to significant (12–29 mm) activities against the selected bacterial species. Similar compounds compared against the same bacterial species also had moderate to significant activities (16–32 mm),^[47] while our previously reported similar compounds had lower activities (12–17 mm) compared to the different bacterial strains.^[30] The metal complexes also exhibited moderate to significant activity overall against all the tested bacterial strains. Compounds **3**, **8**, and **12** were found to be inactive against the *E. coli* (A), *K. pneumoniae* (B), and *S. aureus* (C), respectively. The highest antibacterial activity of 29 mm was found for compound **4** against strain B. The data showed that the antibacterial activity of both ligands is higher than that of their corresponding metal complexes (Figure 10).

3.16.2 | Antifungal bioassay

The sulfonamide ligands and their metal complexes were screened against two fungal strains, *A. niger* (E) and

TABLE 8 Antioxidant results for ligands L¹ and L² and complexes 1–12

Complex	Antiradical activity inhibition (%)	Total iron reducing power (%)	Total phenols (mg GAE/g)
L ¹	55.0	95.5	70.7
L ²	49.0	92.3	86.4
1	46.0	94.3	58.3
2	83.0	88.1	66.7
3	92.0	96.3	29.0
4	94.0	88.1	57.7
5	70.4	96.3	71.0
6	72.0	88.1	69.8
7	59.0	88.1	82.6
8	82.0	96.3	88.1
9	92.7	88.1	77.5
10	94.4	96.3	76.1
11	26.0	88.1	77.8
12	46.9	96.3	72.3

Note. GAE, Gallic Acid Equivalent.

A. flavus (F), as per the literature protocol. The results showed that most compounds had moderate antifungal activity against both fungal strains (Table 7). Both the ligands exhibited good antifungal activities against the selected fungal strains. However, it was observed that most of their complexes had moderate to weak bioactivities. The data further showed that complex **11** demonstrated excellent activity (above 80%) against E and complex **4** had the highest activity for F, while previously reported compounds with same sulfonamide moiety had the lower activity (75%).^[61] It was also noted that most of the transition metal complexes showed less average activity than their corresponding ligands. Only the zinc complex of **L²** had higher activity than its ligand for both the fungal strains (Figure 11).

TABLE 9 Enzyme inhibition results for ligands **L¹** and **L²** and complexes **1–12**

Complex	Enzyme inhibition (%)			
	Protease	Amylase	AChE	BChE
L¹	67	68	56	49
L²	56	47	46	51
1	67	57	57	68
2	76	71	76	76
3	57	56	76	65
4	76	76	76	76
5	87	87	87	87
6	78	71	68	56
7	69	61	49	74
8	76	73	71	64
9	91	67	56	79
10	87	82	57	65
11	85	78	83	68
12	83	86	86	71

Note. AChE, acetylcholine esterase; BChE, butyrylcholinesterase.

3.16.3 | Antioxidant bioassay

Quantitative relationships for different antioxidant activities (DPPH, total phenolic contents, and total iron reducing power) were determined. The relative dependences of antioxidant activities as a result of the comparison of any two values (antiradical activity vs. total iron reducing power, antiradical activity vs. total phenols, and total iron reducing power vs. total phenols) (Figure 12) were determined by interpreting their correlation coefficient as R^2 .^[34]

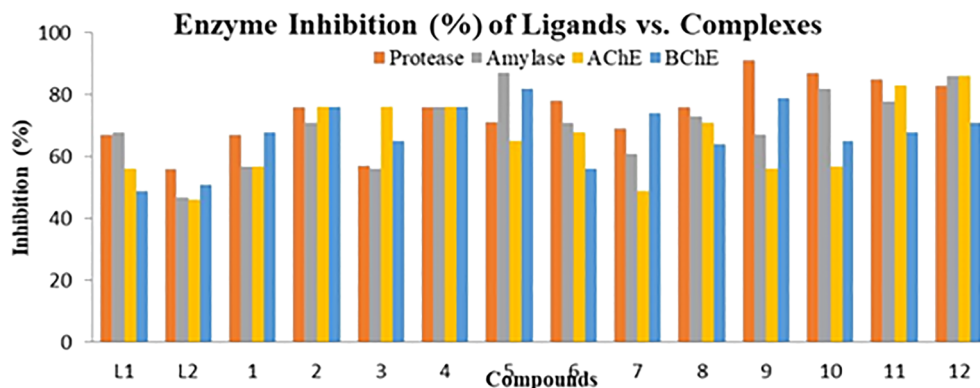
The antiradical scavenging activities of all the synthetic compounds were determined by spectrophotometry, using DPPH as the free radical with gallic acid as the standard. The results show that the entire sample to be quite good at their scavenging ability. The maximum activity (94.4%) was exhibited by compound **10** while the lowest activity (46%) was exhibited by compound **1**, as shown in Table 8.

Phenolic compounds are found to be good antioxidants and phenol-containing compounds have been shown to have good antioxidant properties.^[62] Total phenolic content for the ligands and their complexes was determined as milligram equivalent of gallic acid standard. The highest value of 88.1% was found for compound **8** while the lowest value of just 29% was observed for compound **3**. Total iron reducing power was observed to be significant values varying from 88.1% (**2**, **4**, **6**, **7**, **9**, and **11**) to 96.3% (**3**, **5**, **8**, **10**, and **12**). There was a close relationship between total iron-reducing power and antioxidant activities as per literature reports.^[63]

3.16.4 | Enzyme inhibition results

Enzyme inhibition studies of synthesized products were performed against protease, α -amylase, AChE, and BChE enzymes by taking their absorbance at 400 nm,

FIGURE 13 Enzyme inhibition results for the ligands and their complexes



adopting the standard protocol given in the experimental section. The results revealed that all the synthesized compounds had good enzyme inhibition properties (Table 9), as found for many previously synthesized similar types of compounds.^[64] The protease enzyme showed maximum activity of 91% against compound **9** while α -amylase had a maximum activity of 87% against compound **5**. The AChE enzyme had maximum activity (86%) for compound **12**. The BChE enzyme had maximum activity of 82% against compound **5**. The other remaining compounds also had significant values against all four enzymes (Figure 13).

4 | CONCLUSIONS

Sulfonamide incorporated ligands were prepared by condensing 2-hydroxy-3-methoxybenzaldehyde with 4-aminobenzene-1-sulfonamide and 4-amino-*N*-(3-methyl-2,3-dihydro-1,2-oxazol-5-yl)benzene-1-sulfonamide in an equimolar ratio. The sulfonamide-based ligands acted as bidentate ligands and complexed with transition metals through azomethine-*N* and phenolic-*O*. The compounds were characterized by physical, spectral, and analytical techniques. SC-XRD analysis of **L**¹ revealed its crystals to be monoclinic. Magnetic studies and molecular formula evaluation indicated that the complexes are octahedral in their geometry except for the vanadyl complexes, which showed square planar geometry. The molar conductance confirmed the metal complexes to be nonelectrolytic. All the prepared compounds were subjected to antibacterial, antifungal, antioxidant, and enzyme inhibition studies. The results revealed less significant activities for the synthesized compounds. The biological screening results for the metal complexes showed higher activities than for their respective ligands due to their chelating behavior. The energy gap of HOMO \rightarrow LUMO for **L**¹ was observed to be 0.138 E_h and the global softness value was found to be larger than the global hardness value. The results show that **L**¹ is less stable, therefore it has a stronger tendency to form complexes easily with different metals. Moreover, **L**¹ had a larger dipole moment and β_{tot} compared to urea.

ACKNOWLEDGEMENTS

The authors thank the Higher Education Commission (HEC), Islamabad, Pakistan for financial assistance through NRP project #7800.

CONFLICT OF INTEREST/OPINION

Authors declare no conflict of interest regarding the publication of this paper.

ORCID

Muhammad Khalid  <https://orcid.org/0000-0002-1899-5689>

REFERENCES

- [1] C. T. Prabhakara, S. A. Patil, S. S. Toragalmath, S. M. Kinnal, P. S. Badami, *J. Photochem. Photobiol.* **2016**, *157*, 1.
- [2] Z. H. Chohan, A. U. Shaikh, C. T. Supuran, *J. Enzyme Inhib. Med. Chem.* **2006**, *21*, 733.
- [3] M. N. Tahir, M. Khalid, A. Islam, S. M. A. Mashhadi, A. A. C. Braga, *J. Mol. Struct.* **2017**, *1127*, 766.
- [4] (a) L. H. Abdel-Rahman, M. S. Adam, A. M. Abu-Dief, H. Moustafa, M. Basha, A. H. Aboria, B. S. Al-Farhan, H. E. Ahmed, *Appl. Organomet. Chem.* **2018**, *32*, 4527. (b) A. Desoky, M. Mohamad, M. J. A. Abualreish, A. M. Abu-Dief, *J. Mol. Liq.* **2019**, *290*, 111162.
- [5] A. Ahlawat, P. Khatkar, V. Singh, S. Asija, *Res. Chem. Intermed.* **2018**, *44*, 4415.
- [6] M. Rajasekar, S. Sreedaran, R. Prabu, V. Narayanan, R. Jegadeesh, N. Raaman, A. K. Rahiman, *J. Coord. Chem.* **2010**, *63*, 136.
- [7] N. Vamsikrishna, M. P. Kumar, G. Ramesh, N. Ganji, S. Daravath, *J. Chem. Sci.* **2017**, *129*, 609.
- [8] S. H. Sumrra, M. Ibrahim, S. Ambreen, M. Imran, M. Danish, F. S. Rehmani, *Bioinorg. Chem. Appl.* **2014**, *2014*, 1.
- [9] B. S. Kusmariya, A. Tiwari, A. P. Mishra, G. A. Naikoo, *J. Mol. Struct.* **2016**, *1119*, 115.
- [10] S. H. Sumrra, M. Hanif, Z. H. Chohan, M. S. Akram, J. Akhtar, S. M. Alshehri, *J. Enzyme Inhib. Med. Chem.* **2016**, *31*, 590.
- [11] S. G. Yiase, S. O. Adejo, J. A. Gbertyo, J. Edeh, *J. Appl. Chem.* **2014**, *7*, 4.
- [12] M. Dyba, N. Tarasova, C. Michejda, *Curr. Pharm. Des.* **2005**, *10*, 2311.
- [13] Z. H. Chohan, A. U. Shaikh, M. M. Naseer, *Appl. Organomet. Chem.* **2006**, *20*, 729.
- [14] L. H. Abdel-Rahman, R. M. El-Khatib, L. A. E. Nassr, A. M. Abu-Dief, F. E. D. Lashin, *Spectrochim. Acta - Part A.* **2013**, *111*, 266.
- [15] Y. L. Sang, X. S. Lin, X. C. Li, Y. H. Liu, X. H. Zhang, *Inorg. Nano-Metal Chem.* **2017**, *47*, 86.
- [16] Ü. Ö. Özdemir, P. Güvenç, E. Şahin, F. Hamurcu, *Inorg. Theor. Chim. Acta* **2009**, *362*, 2613.
- [17] S. Mondal, T. K. Mondal, Y. Rajesh, M. Mandal, C. Sinha, *Polyhedron* **2018**, *151*, 344.
- [18] I. Kaur, A. Khajuria, P. Ohri, P. Kaur, K. Singh, *Sensors Actuat. B. Chem.* **2018**, *268*, 29.
- [19] S. H. Sumrra, S. Kausar, M. A. Raza, M. Zubair, M. N. Zafar, M. A. Nadeem, E. U. Mughal, Z. H. Chohan, F. Mushtaq, U. Rashid, *J. Mol. Struct.* **2018**, *1168*, 202.
- [20] B. S. Kusmariya, A. Tiwari, A. P. Mishra, G. Ahmad, *J. Mol. Struct.* **2016**, *1119*, 115.
- [21] L. Rodríguez, E. Labisbal, A. S. Pedrares, J. A. G. Vázquez, J. Romero, A. Sousa, *Inorg. Chim. Acta* **2010**, *363*, 1284.
- [22] Z. H. Chohan, H. A. Shad, F. H. Nasim, *Appl. Organomet. Chem.* **2009**, *23*, 319.
- [23] S. Yasmeen, S. H. Sumrra, M. S. Akram, Z. H. Chohan, *J. Enzyme Inhib. Med. Chem.* **2017**, *32*, 106.
- [24] M. S. Nair, R. S. Joseyphus, *Spectrochim. Acta-Part A.* **2008**, *70*, 749.

- [25] M. Shahid, M. Salim, M. Khalid, M. N. Tahir, M. U. Khan, A. C. Braga, *J. Mol. Struct.* **2018**, *1161*, 66.
- [26] K. Dhahagani, M. P. Kesavan, G. Gangatharan, V. Kumar, L. Ravi, G. Rajagopal, G. J. Rajesh, *Mater. Sci. Eng. C* **2018**, *90*, 119.
- [27] M. Szafran, A. Katrusiak, *J. Mol. Struct.* **2007**, *827*, 56.
- [28] C. Ecjhaio, P. Jogi, K. Mounika, M. Padmaja, C. Gyanakumari, *Elec. J. Chem.* **2011**, *8*, 1662.
- [29] (a)L. H. Abdel-Rahman, R. M. El-Khatib, L. A. E. Nassr, A. M. Abu-Dief, M. Ismael, A. A. Seleem, *Spectrochim. Acta-Part A* **2014**, *117*, 366. (b)L. H. Abdel-Rahman, A. M. Abu-Dief, R. M. El-Khatib, S. M. Abdel-Fatah, *J. Bioorg. Chem.* **2016**, *69*, 140.
- [30] S. H. Sumrra, A. Suleman, Z. H. Chohan, M. N. Zafar, M. A. Raza, T. Iqbal, *Russ. J. Gen. Chem.* **2017**, *87*, 1281.
- [31] (a)A. M. Abu-Dief, L. H. Abdel-Rahman, M. R. Shehata, A. A. Hassan Abdel-Mawgoud, *J. Phy. Org. Chem.* **2019**, *32*, e4009. (b)A. M. Abu-Dief, H. M. El-Sagher, M. R. Shehata, *Appl. Organomet. Chem.* **2019**, *33*, 4943.
- [32] S. K. Tadavi, J. D. Rajput, S. D. Bagul, A. A. Hosamani, J. N. Sangshetti, R. S. Bendre, *Res. Chem. Intermed.* **2017**, *43*, 4863.
- [33] A. Matkowski, M. Piotrowska, *Fitoterapia* **2006**, *77*, 346.
- [34] M. A. Raza, M. Danish, M. Mushtaq, S. H. Sumrra, Z. Saqib, S. Rehman, *Open Chem.* **2017**, *1*, 371.
- [35] R. N. Prabhu, J. LakshmiPraba, *Transition Met. Chem.* **2017**, *42*, 579.
- [36] N. K. Singh, P. Tripathi, M. K. Bharty, A. K. Srivastava, S. Singh, R. J. Butcher, *Polyhedron* **2010**, *29*, 1939.
- [37] F. Chen, M. S. Askari, X. Ottenwaelder, *Inorg. Chim. Acta* **2013**, *407*, 25.
- [38] S. A. Patil, C. T. Prabhakara, B. M. Halasangi, S. S. Toragalmath, P. S. Badami, *Spectrochim. Acta-Part A* **2015**, *137*, 641.
- [39] I. Rama, R. Selvameena, *J. Chem. Sci.* **2015**, *127*, 671.
- [40] K. Singh, S. Raparia, S. Raparia, *Eur. Chem. Sci.* **2016**, *5*, 92.
- [41] K. Mohanan, N. Subhadrambika, R. S. Joseyphus, S. S. S. Swathy, V. P. P. Nisha, *J. Saudi Chem. Soc.* **2016**, *20*, 379.
- [42] S. Chandra, P. Pipil, *Open J. Inorg. Chem.* **2014**, *4*, 30.
- [43] H. Keyypour, M. Shayesteh, M. Rezaeivala, F. Chalabian, Y. Elerman, O. Buyukgungor, *J. Mol. Struct.* **2013**, *1032*, 62.
- [44] M. Amjad, S. H. Sumrra, M. S. Akram, Z. H. Chohan, *J. Enzyme Inhib. Med. Chem.* **2016**, *31*, 88.
- [45] S. Jana, A. Bhattacharyya, B. N. Ghosh, K. Rissanen, S. Herrero, R. J. Aparicio, S. Chattopadhyay, *Inorg. Chim. Acta* **2016**, *453*, 715.
- [46] A. N. M. A. Alaghaz, H. A. Bayoumi, Y. A. Ammar, S. A. Aldhlmani, *J. Mol. Struct.* **2013**, *1035*, 383.
- [47] Z. H. Chohan, H. A. Shad, C. T. Supuran, *J. Enzyme Inhib. Med. Chem.* **2012**, *27*, 58.
- [48] R. K. Jain, A. P. Mishra, *J. Saudi Chem. Soc.* **2016**, *20*, 127.
- [49] V. Jaishree, N. Ramdas, J. Sachin, B. Ramesh, *J. Saudi Chem. Soc.* **2012**, *16*, 371.
- [50] I. P. Ejidike, P. K. Ajibade, *Molecules* **2015**, *20*, 9788.
- [51] S. Naseem, M. Khalid, M. N. Tahir, M. A. Halim, A. A. C. Braga, M. M. Naseer, Z. Shafiq, *J. Mol. Struct.* **2017**, *1143*, 235.
- [52] I. K. Cikla, S. Guveli, M. Yavuz, T. Bal-Demirci, B. Ulkuseven, *Polyhedron* **2016**, *105*, 104.
- [53] E. D. Glendening, C. R. Landis, F. Weinhold, *Wiley Interdiscip. Rev. Comput. Mol. Sci.* **2012**, *2*, 1.
- [54] I. Khosravi, F. Hosseini, M. Khorshidifard, M. Sahihi, H. A. Rudbari, *J. Mol. Struct.* **2016**, *1119*, 373.
- [55] H. Ebrahimi, J. S. Hadi, H. S. Al-Ansari, *J. Mol. Struct.* **2013**, *1039*, 37.
- [56] M. Homocianu, A. Airinei, C. H. MirelaIpate, *J. Mol. Liq.* **2019**, *281*, 141.
- [57] N. Prabavathi, A. Nilufer, V. Krishnakumar, *Spectrochim. Acta-Part A* **2013**, *114*, 449.
- [58] S. H. Sumrra, F. Mushtaq, M. Khalid, M. A. Raza, M. F. Nazar, B. Ali, A. A. C. Braga, *Spectrochim. Acta-Part A* **2018**, *190*, 197.
- [59] P. Jayaseelan, E. Akila, M. U. Rani, R. Rajavel, *J. Saudi Chem. Soc.* **2016**, *20*, 625.
- [60] S. Sumathi, P. Tharmaraj, C. D. Sheela, R. Ebenezer, *J. Coord. Chem.* **2011**, *64*, 1673.
- [61] S. Rani, S. H. Sumrra, Z. H. Chohan, *Russ. J. Gen. Chem.* **2017**, *87*, 1834.
- [62] M. N. Arshad, A. A. M. Al-Dies, A. M. Asiri, M. Khalid, A. S. Birinji, K. A. A. Amry, A. A. C. Braga, *J. Mol. Struct.* **2017**, *1141*, 142.
- [63] J. B. Mohankumar, A. J. Gladius, M. Velvizhi, *J. Food Med. Res.* **2017**, *5*, 180.
- [64] A. A. M. Abdel-Aziz, A. Anjali, A. S. El-Azab, M. E. A. Hammouda, M. A. El-Sherbeny, C. T. Supuran, *Bio-org. Chem.* **2019**, *84*, 260.

SUPPORTING INFORMATION

Additional supporting information may be found online in the Supporting Information section at the end of this article.

How to cite this article: Sumrra SH, Hassan AU, Imran M, et al. Synthesis, characterization, and biological screening of metal complexes of novel sulfonamide derivatives: Experimental and theoretical analysis of sulfonamide crystal. *Appl Organometal Chem.* 2020;e5623. <https://doi.org/10.1002/aoc.5623>